New experiments with the Short-Lived Isotope Counting System

Mark Yuly, Andrew Bo, Olivia Ocker, Sam Plymale, Dante Vara, Charlie Freeman, Stephen Padalino.

I. The history of and motivation for Short-lived Isotope Counting System (SLICS)

Over the past ten years the Short-Lived Counting System (SLICS) has been designed, built, and tested [1-14] by a collaboration of physicists and engineers from Houghton University, SUNY Geneseo and the Laboratory for Laser Energetics (LLE) as a tool for making nuclear activation measurements using ultra-fast high-power lasers. It is now a standard diagnostic for both the OMEGA-60 and OMEGA-EP target chambers, and has been used to help settle a disagreement on the OMEGA deuterium-deuterium neutron yield [15], to resolve the discrepancy between previous measurements of the ^{9}Be(n,α)^{6}He cross section at 14.1 MeV [16], and a paper has been published describing the detector system and the "shakedown cruise" experiment [17] measuring ^{7}Li(d,p)^{8}Li with OMEGA-EP accelerated deuterons.

One of the unique features of these fast-pulse high power laser systems, such as the OMEGA-EP and OMEGA-60 lasers at LLE, is that they can initiate a truly stupendous number of nuclear reactions in an extremely short period of time. For example, in less than one nanosecond 2×10^{14} reactions occur for inertial confinement fusion (ICF) or 10^{12} high-energy ions are generated using target normal sheath acceleration (TNSA). This fact implies that there may be measurements that can be made using these techniques that would be difficult or even impossible using traditional accelerator techniques. In particular, activation experiments in which radioactive product nuclei are created in a very short time and counted long after (in relative terms) the laser shot have many advantages over traditional accelerator-based measurements which require hundreds or more beam pulses over weeks or months.

Over time, as we thought of more and more ways SLICS could be used, the scope of possible experiments was expanded. The initial motivation for developing SLICS was to investigate the previously unmeasured ^{3}H(t,γ)^{6}He reaction at thermonuclear energies using ICF. It quicky became evident that ICF allows other light ion reactions to also be examined using SLICS as long as they produce radioactive products. Later, when MTW and OMEGA-EP experiments used TNSA to accelerate light ions, it was apparent that reactions at higher ion energies could also be studied. Finally, the initial neutron experiments intended to test the SLICS system made it clear that neutron-induced reactions could also be studied.

The versatility of the SLICS detector for so many types of nuclear measurements makes it difficult to concisely describe the motivation for developing the detector, because the different types of experiments are so closely intertwined. Table 1 attempts to describe and differentiate the motivations for constructing both the TNSA tritium platform and the SLICS detector, and disconnect them from the motivations for carrying out any one particular measurement using ICF or TNSA.

In Table 1, the green columns refer to experiments using the TNSA platform to accelerate ions, particularly tritons, to energies in the range 1-20 MeV. The orange columns refer to experiments involving either ICF neutrons or thermonuclear light-ion reactions at ion temperatures less than about 20 keV occurring in the ICF implosion. The topmost horizontal section describes the advantages and disadvantages of TNSA and ICF as techniques for measuring these reaction cross sections, the middle horizontal section gives details, motivations and possible examples for experiments using SLICS with TNSA and ICF. The bottom horizontal section gives the same information for other techniques than activation which therefore require other kinds of detectors than SLICS.

Table 1. The advantages, disadvantages and problems associated with TNSA and ICF experiments using SLICS.

Detector/Source		**TNSA**	**ICF**	
Technique	Properties	Reaction energies > 100 keV	2.45 MeV, 14.1 MeV	Reaction energies < 30 kev
	Advantages	Ions in fast ~1 ns pulse – small cross sections	n in fast ~1 ns pulse	Reactions in fast ~1 ns pulse
	Problems	Not monoenergetic – deconvolution required		Capturing reaction products

		Tritium reactions	**Other light ions (p, d, ^{3}He, ^{4}He)**	**Neutron reactions**	**Thermonuclear reactions (p, d, t, ^{3}He, ^{4}He)**
SLICS	Properties	Detect radioactive reaction products 20 ms < $t_{1/2} \lesssim$ 1 min		Detect radioactive reaction products 20 ms < $t_{1/2} \lesssim$ 1 min	
	Motivation	No tritium accelerators! Nucleosynthesis >100 keV Target nuclei Z $\lesssim$ 12 ($t_{1/2}$)	Nucleosynthesis >100 keV Target nuclei Z $\lesssim$ 12 ($t_{1/2}$)	Calibration Reactor nuclear data	No tritium accelerators! Thermonuclear plasma! Nucleosynthesis at <30 keV!
	Examples	^{3}H(t,γ)^{6}He ^{7}Li(t,n)^{9}Be ^{7}Li(t,α)^{6}He ^{9}Be(t, α)^{8}Li	^{7}Li(d,p)^{8}Li ^{11}B(d,p)^{12}B ^{7}Li(^{3}He, p)^{9}Li	^{9}Be(n,α)^{6}He ^{11}B(n,α)^{8}Li	^{3}H(t,γ)^{6}He ^{9}Be(t,γ)^{12}B ^{6}Li(t,p)^{8}Li ^{10}B(t,p)^{12}B ^{7}Li(t,α)^{6}He ^{11}B(d,p)^{12}B ^{9}Be(t,α)^{8}Li

		Tritium reactions	**Other light ions (p, d, ^{3}He, ^{4}He)**	**Neutron reactions**	**Thermonuclear reactions**
Other techniques/ detectors	Properties	Detect prompt radiation	Detect prompt radiation	Detect prompt radiation	Detect prompt radiation
	Motivation	No tritium accelerators! Nucleosynthesis >100 keV Any target nuclei	Nucleosynthesis >100 keV Any target nuclei	Realm of nTOF detectors	Realm of Cherenkov gamma detectors, TPIE and proton spectrometers
	Examples	^{7}Li(t,n_{tot})			

For both ICF and TNSA, the biggest advantage is that the reactions all occur in < 1 ns, eliminating the need for a pulsed beam, maximizing the number of reaction products produced since they do not have time to decay while being created, and reducing the background since all the reaction products can be counted within a few half-lives. Very few cross sections have been measured at the 10-20 keV energy scale because it is so difficult with particle accelerators. ICF allows these cross sections to be measured inherently, in the same plasma environment that would exist in a start of the early universe. Moreover, since there are currently no accelerators that accelerate tritium, another motivation for both techniques is that they allow never-before-measured tritium reactions to be studied.

Instead of activation, nuclear experiments ordinarily measure the prompt radiation from the nuclear reactions directly. The problem with this is that for ICF and TNSA all of the other prompt radiation and the EMF also is emitted in < 1 ns, meaning that only TOF or integrating detectors (like CR-39 or image plates) can be used.

Ultimately, the motivation for both the TNSA platform and SLICS is that they are versatile instruments that can be used to make a large number of measurements – covering a huge range of incident ion energies and reactions on a large number of targets, not limited to low-Z, many of which have never been measured or measured. For example, the ^{9}Be(t, α)^{8}Li reaction, which is important for nucleosynthesis models [18], could be measured at energies <20 keV using ICF and > 100 keV using TNSA, and has in the past only been measured in ~1970 for the range of 0.5 – 2 MeV. The contribution to our understanding of nucleosynthesis would be the motivation for making this particular measurement, especially at the low-energy obtainable using ICF, but as a motivation for creating the SLICS this would only be one of a very large number of important measurements that could be conceivably made.

Our previous report, from the summer of 2025, described how the SLICS detector was redesigned to fit inside a ten-inch manipulator (TIM) so that it could be inserted into the OMEGA-60 or OMEGA-EP target chambers. Section II of this report describes the first test of this new design, which was a TNSA experiment in August 2026 using OMEGA-EP to accelerate deuterons into a thin natural lithium target. Analysis of this experiment was carried out over the academic year. Section III of the report describes another experiment, carried out during the summer of 2026, using the 1.7 MV Pelletron accelerator at SUNY Geneseo to study the feasibility of an experiment to measure the fraction of product nuclei that would implant or stick to the SLICS detector in an ICF experiment.

II. First test of the TIM-based SLICS in an OMEGA-EP TNSA Experiment

The first test of the newly redesigned SLICS detector was a two shot-day campaign using OMEGA-EP on August 12 and 14, 2025. In this experiment, as shown in Figure 1, alternating sidelighter and backlighter laser shots with nominally identical laser parameters (energy, width) struck either a bare or titanium coated 25 µm thick stainless steel substrate onto which deuterium or hydrogen had been adsorbed.

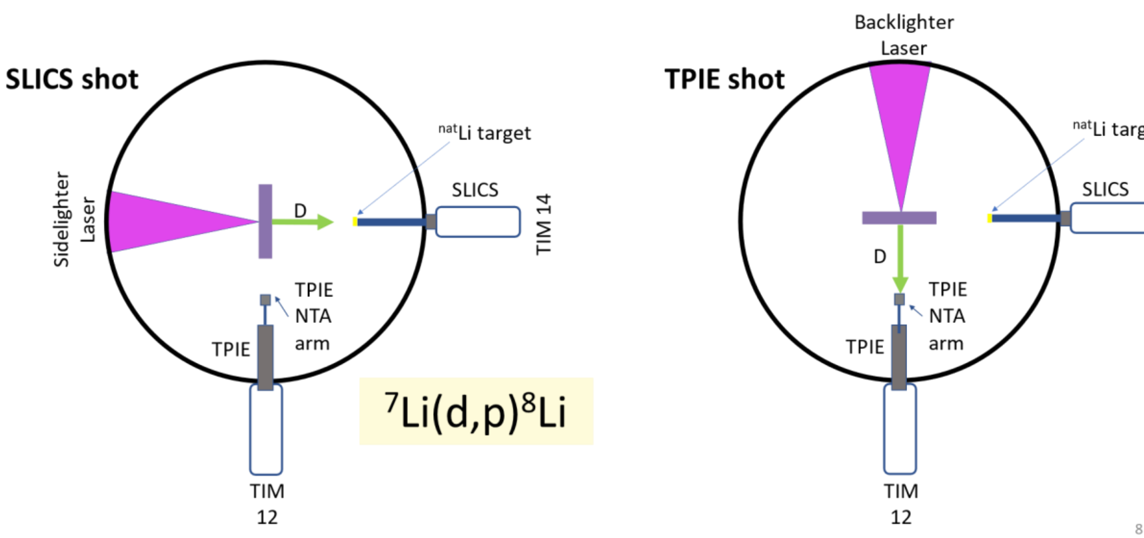

Figure 1. Experimental Layout for OMEGA-EP TNSA experiment. First (left) the sidelighter laser strikes the deuterated laser target to produce a pulse of TNSA deuterons which then strike the lithium nuclear target on the end of the SLICS phoswich detector to produce ^{8}Li via the ^{7}Li(d,p)^{8}Li reaction. These laser shots alternate with backlighter laser shots (right) with the deuterated laser target rotated by 90 degrees to point at the Thomson Parabola (TPIE) detector in order to measure the incident deuteron energy spectrum.

The laser target was rotated 90° between the sidelighter and backlighter shots so that the TNSA accelerated deuterons and protons would be directed toward either SLICS for sidelighter shots or the Thomson Parabola (TPIE) for backlighter shots. The TPIE was used to measure the energy distribution for each ion species, which ostensibly should be the same for the corresponding sidelighter shot with the same laser parameters. The TPIE measurement could be compared to the SLICS particle time-of-flight (pTOF) measurement, which gave the overall time-of-flight for all ions striking the SLICS nuclear target, but could not separate them by ion species.

For sidelighter shots, the deuterons and protons struck a thin lithium film deposited onto a 25 thick stainless-steel substrate. When initially formed using physical vapor deposition, these films were about 2 to 15 µm thick lithium metal, which later was allowed to oxidize in air. The ^{7}Li(d,p)^{8}Li reaction that occurred when the TNSA accelerated deuterons struck the natural lithium target produced ^{8}Li, which decays by beta emission. These beta particles were then identified and counted by the SLICS detector as a function of time after the laser shot. Fitting the integral of the resulting ^{8}Li decay curve allowed the yield of ^{8}Li formed by the TNSA deuterons to be measured.

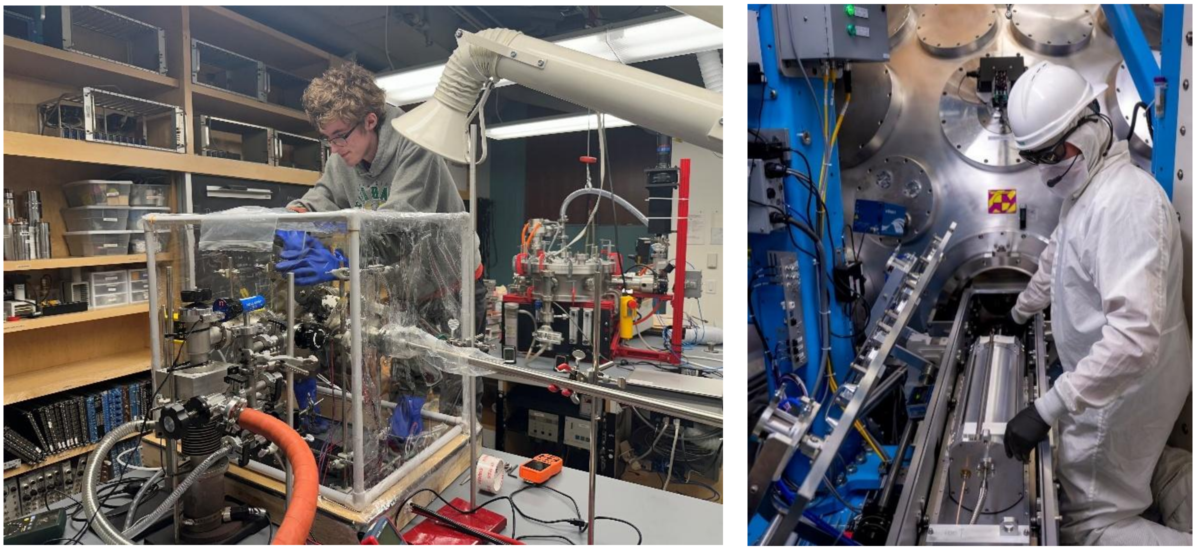

Figure 2. (Left) Houghton University undergraduate student Andrew Bo created the thin-film lithium targets using a specially-designed lithium deposition chamber that allows the highly reactive lithium to be handled in an argon atmosphere. Andrew will be entering the Physics PhD program at LeHigh University. (Right) The SLICS detector being inserted in to the TIM.

Table 2 presents a list of the OMEGA-EP laser shots and the parameters associated with each shot. Initially, the Li nuclear target, attached to the end of the SLICS detector, was positioned at a distance of 35 cm from the laser target. The initial "half-power" TPIE shot (43416) and SLICS shot (43417) seemed to perform well. For the 43417 SLICS shot, a ^{8}Li beta decay spectrum was obtained.

Unfortunately, for the next two SLICS shots, no ^{8}Li decays were detected. After much puzzlement, it was decided that the only possible explanation was that the Lithium target was gone, which is what was discovered when the target was removed. Figure 3 shows Target 34 before inserting into the detector and after it was removed. All of the lithium coating, with the exception of the lithium in the "shadow" of the pTOF detector, was "sandblasted" off the substrate.

This target was replaced with Target 30 and moved back to a distance of 51 cm from the laser target for the next two SLICS laser shots and their corresponding TPIE shots. After the first, shot 43424, the lithium target was removed and examined. While it appeared that at least some amount of lithium remained on the target, bits of material could be seen embedded in the lithium, presumably bits of the laser target. The next SLICS shot also detected ^{8}Li decay, so it appeared that moving back reduced the degradation of the target. Interestingly, analysis of the number of ^{8}Li decays detected was consistent with no reduction in the amount of lithium.

On the next shot day, the lithium target was moved back to 100 cm from the laser target, and replaced with a fresh target (Target 35) which, unfortunately, had not had its thickness measured. Once again, ^{8}Li was detected after the first SLICS laser shot (shot 43430) but not in the following two shots (43433, 43436) even though after each of these shots the lithium target was examined and appeared to be intact. Later, after the target was removed, close examination as in Figure 4 showed shards of material embedded in the lithium, although it appeared that lithium was still present. One possible explanation for why ^{8}Li was not detected even though there appeared to be lithium on the target is that material expelled from the laser target after the shot coated the lithium target, preventing TNSA deuterons from later shots from reaching the lithium.

Table 2. List of OMEGA-EP shots and shot parameters. SL=sidelighter, BL=backlighter. The brown rows are good SLCIS shots from which the ^{8}Li yield was extracted.

OMEGA-EP Shot No.	OMEGA-EP Laser	Laser Target	Detector	Energy (J)	Li nuclear target No.	Li nuclear target thickness (um)	Distance to Li target (cm)	First trigger delay (s)	^{8}Li formed
43416	BL	D	TPIE	497					
43417	SL	D	SLICS	364	34	4.61	35	2	Y
43418	BL	D	TPIE	746					
43419	SL	D	SLICS	724	34	4.61	35	3	N
43420	BL	D	TPIE	479					
43421	SL	D	SLICS	366	34	4.61	35	5	N
43422	NULL								
43423	BL	D	TPIE	478					
43424	SL	D	SLICS	370	30	6.13	51	0.4	Y
43425	BL	D	TPIE	365					
43426	SL	D	SLICS	365	30	6.13	51	1.6	Y
43429	BL	D	TPIE	520.9					
43430	SL	D	SLICS	382.8	35	?	100	0.25	Y
43431	BL	D	TPIE	363.7					
43432	NULL								
43433	SL	D	SLICS	749.4	35	?	100	No data acquisition	
43434	BL	D	TPIE	713.9					
43435	NULL								
43436	SL	D	SLICS	713.9	35	?	100		N (tiny)
43437	BL	D	TPIE	369.5					
43438	SL	D	SLICS	139	38	14.81	100	0.09	Y
43439	SL	H	SLICS	137	37	?	100		
43440	BL	D	TPIE	134.7					
43441	SL	D	SLICS	724	33	2.01	100	0.12	Y

For the final two SLICS shots, fresh lithium targets were used and both shots yielded a measurable amount of ^{8}Li, leading to the conclusion that each lithium target can only be used for a single laser shot. In the end, there were six useable SLICS laser shots, with four corresponding TPIE shots, from which ^{8}Li yields could be obtained.

In order to measure the ^{7}Li(d,p)^{8}Li yield, events corresponding to beta decay were selected from the 2D dE-E histogram for each SLICS laser shot. The location of this selected region was used with a GEANT simulation of the predicted detector response in order to determine the efficiency of the detector for the selected region, which, for the selection region drawn on the 2D histogram shown in Figure 5 for OMEGA-EP shot 43424, was determined to be 24.4% ± 2%.

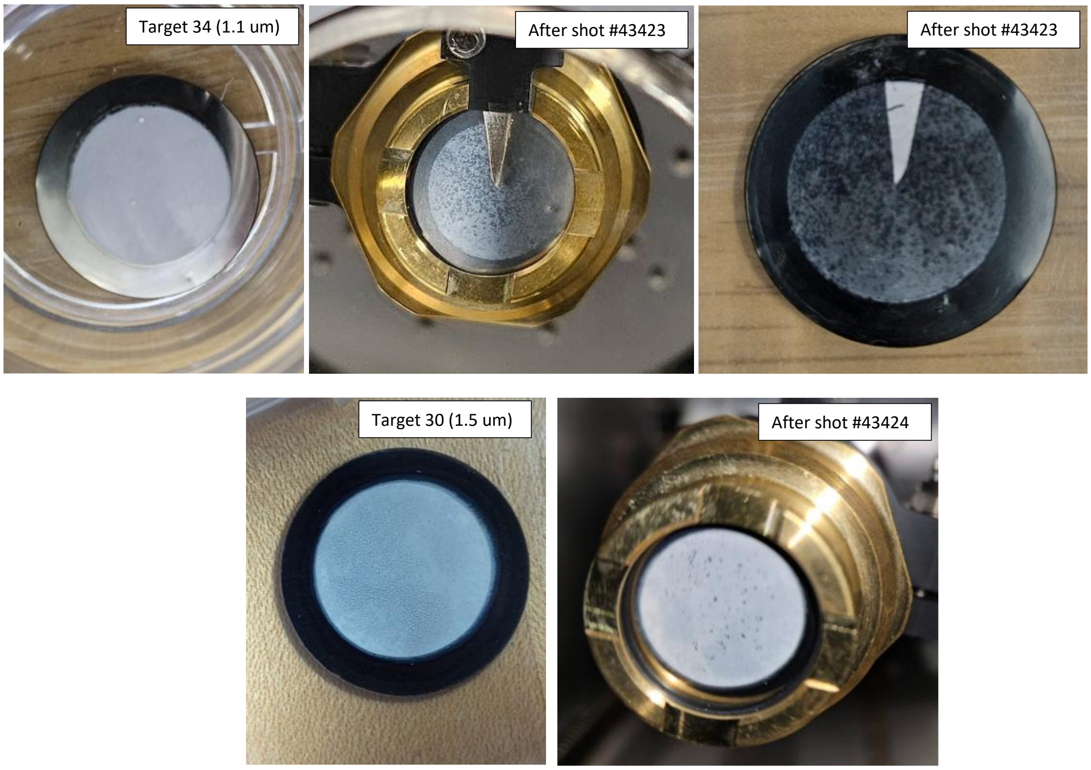

Figure 3. The first Li target used (Target 34) prior to insertion into the SLICS detector (top left) and after shot 43423 (top center), and after removal from the SLICS detector (top right). Most, if not all, of the lithium has been "sandblasted" off the stainless-steel substrate. The gold coating on the pTOF detector has also disappeared, leaving the aluminum coating with what appear to be bits of shrapnel embedded in it. Lithium remains on the substrate where it was shadowed by the pTOF detector. The second target used in the experiment (Target 30) is shown before (bottom left) and after laser shot 43424 (bottom right). For this shot, the Li target was moved back to a distance of 51 cm from the laser target. Nonetheless, there is evidence of damage to the lithium coating, and bits of material appear to be stuck in the surface.

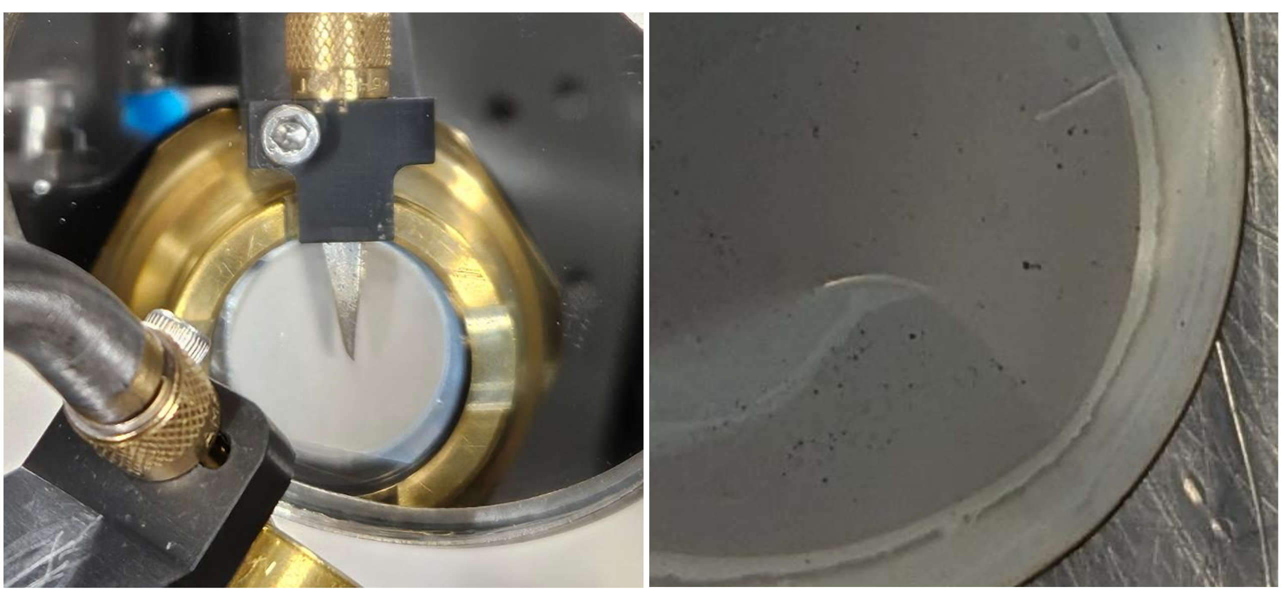

Figure 4. Target 35 after shot 43430 (left) and a close-up after being removed after shot 43436 (right). Although superficial examination did not reveal damage, after the target was removed bits of material could be seen embedded in the lithium.

The events in the selected region were then plotted as a function of time, as shown in Figure 5. For an unknown reason, for shot 42424 the digitizer did not begin triggering immediately after the shot, but about 0.5 s after the shot. The number of events as a function of time was plotted from this time forward to obtain a decay curve which was then integrated to get a growth curve. The growth curve was fitted with two exponential terms and a linear background term,

$$N = P_0(1 - e^{-P_1 t}) + P_2(1 - e^{-P_3 t}) + P_4 t. \quad (1)$$

For one of the exponentials, the half-life was fixed to 838.79 ms, the ^{8}Li decay half-life. It was found that a good fit could not be obtained for most shots using only a single activation component.

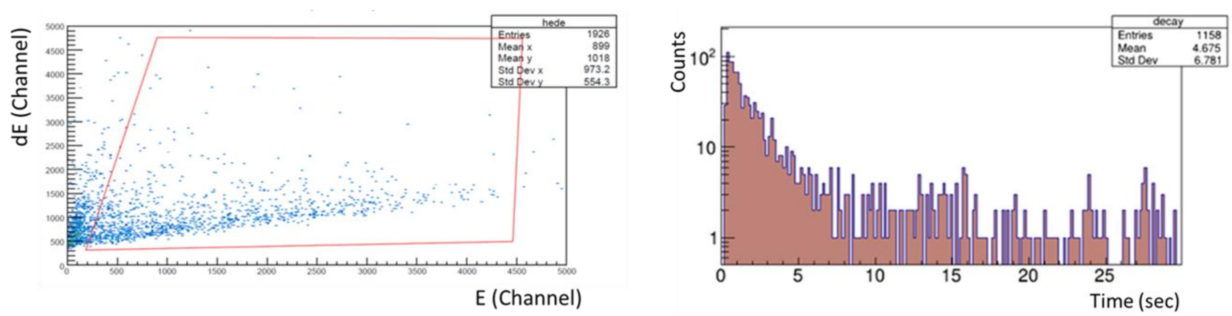

Figure 5. 2D dE-E histogram (left) for OMEGA-EP shot 42424. The events inside the red quadrilateral were histogrammed as a function of time (right) to obtain the decay curve, which was integrated to create the growth curve.

Figure 6 shows the results of the fits for several different laser energies. The reason for the unexpected small "bumps" in the growth curves, clearly evident in the residuals plot, is unknown. It is interesting that both the linear background and the "other" activation do not appear in the 139 J laser shot and seem to grow as the laser energy increases. This would indicate that something is being activated with a half-life between 6.5 and 13 s having an energy threshold that is higher than most deuterons produced by a 139 J laser pulse.

Table 3 shows the overall results of the fits to each of the six OMEGA-EP TNSA laser shots directed at the SLICS detector. Two of the shots could not be used for further analysis: 43430 because the Lithium target thickness was never measured, and 43438 because no TPIE data were collected for a laser shot energy of 139 J.

The number of ^{8}Li detected, determined using the fit to the growth curve with a fixed 838.79 ms half-life, was then used to determine the total yield of ^{8}Li by correcting for the delay in triggering the digitizer ("Integration delay" in Table 3) and the detector efficiency.

The predicted yield for each laser shot was calculated using the deuteron energy spectra from TPIE shots at approximately the same energy. This is problematic, however, since the energy distribution is not consistent shot-to-shot even for the same laser parameters. Figure 7 shows the deuteron energy distribution measured for laser shots of roughly the same energy. The shape of the distribution is usually similar, but the overall normalization can vary by a factor of two.

In order to calculate the predicted ^{8}Li yield, the integral

$$Y = \frac{17}{18} \int \sigma(E)\, N_t \frac{d^2 N_i}{d\Omega\, dE}(E)\, \Delta\Omega\, dE$$

was evaluate numerically, using the ENDF values for the ^{7}Li(d,p)^{8}Li total cross sections $\sigma(E)$ as a function of energy, the lithium target thickness N_t measured at SUNY Geneseo, the solid angle $\Delta\Omega$, and the TPIE-measured deuteron energy distribution $d^2N_i/d\Omega\, dE$ for a similar laser shot. This calculation assumes that the target is thin enough to neglect the energy loss of the deuterons as they traverse the target.

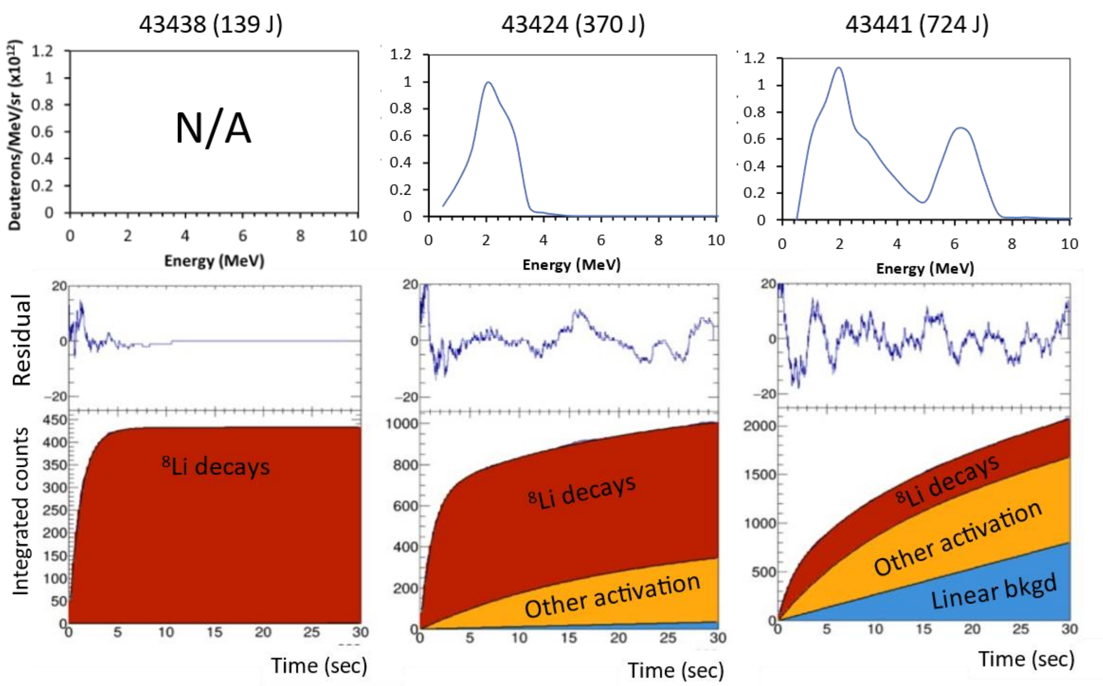

Figure 6. Growth curve plots (bottom), fit residuals (middle), and corresponding TPIE deuteron energy spectra for OMEGA-EP shots at three different laser energies: shot 43438 (139J) (left), 43424 (370J) (center) and 43441 (724J) (right). In each case, the events inside the red quadrilateral shown in Figure 5 were histogrammed at a function of time and the resulting decay curves were integrated to obtain the growth curves (bottom row). Each growth curve was fit with Equation XX to obtain the number of ^{8}Li detected (red area). The blue shaded area indicates the contribution from the background, and the yellow the decay of an unknown activation isotope, which apparently was not activated at the low deuteron energies present in a 139J laser shot.

Table 3. Results of the fits used to determine the number of ^{8}Li created in each laser shot.

OMEGA-EP Shot No.	Laser Energy (J)	Integration Delay (s)	^{8}Li number detected ($t_{1/2}$ = 838.79 ms)	Other number detected	Other λ (s^{-1})	Other $t_{1/2}$ (s)	Background (s^{-1})
43417	364.0	2.00	505.8 ± 4.4	481.9 ± 98.4	0.071 ± 0.013	9.8 ± 1.8	8.4 ± 2.4
43424	370.0	0.50	659.2 ± 3.7	385.6 ± 134.7	0.056 ± 0.015	12.4 ± 3.3	1.1 ± 2.6
43426	365.0	1.60	338.6 ± 4.0	292.1 ± 213.2	0.053 ± 0.030	13.1 ± 7.4	1.4 ± 4.2
43430	382.8	0.25	175.8 ± 2.3	112.2 ± 13.7	0.102 ± 0.015	6.8 ± 0.1	3.7 ± 0.4
43438	139.0	0.09	431.6 ± 0.001	0 ± 0.1			0
43441	724.0	0.12	392.4 ± 4.8	918.6 ± 31.0	0.104 ± 0.004	6.7 ± 0.3	26.8 ± 1.0

In order to test this, another calculation was carried out in which the rate of energy loss in lithium carbonate (from SRIM) was used to account for the energy loss in each "slice" of the target. For the thickest target that was manufactured for this experiment (but not used), approximately 6.33×10^{19} atoms/cm^2, energy loss in the target resulted in a correction of about 24%. For the targets for which we obtained data in this experiment, the correction is at most 7%. The 17/18 is the fraction of the target that was not covered by the pTOF detector.

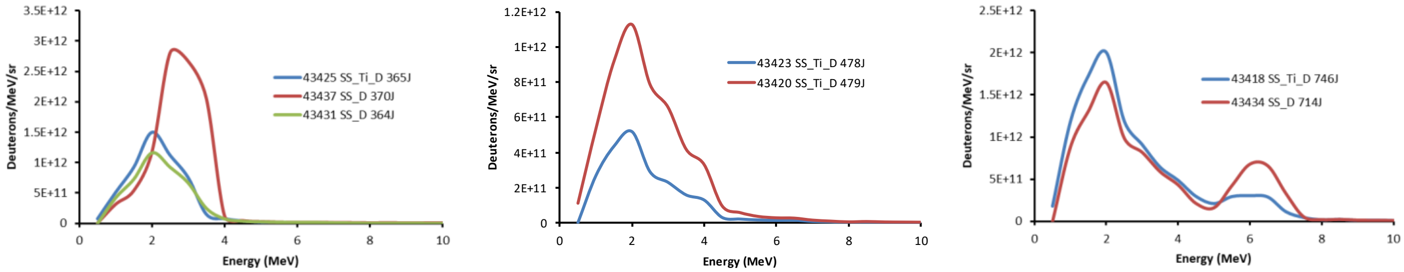

Figure 7. Deuteron energy distributions measured using TPIE for laser shots with energies near 370 J (left), 480 J (center) and 730 J (right). While the shape is often similar, the overall normalization can vary by a factor of two.

The TPIE Thomson parabola can measure the energy distribution of each ion species, but not for the same SLICS shot as when deuterons hit the lithium target. The pTOF detector can measure the energy distribution actually striking the lithium target during a SLICS shot, but cannot separate the different ion species. In Figure 8 the left plot shows the Thomson parabola-measured deuteron and proton energy spectra for the 714 J TPIE laser shot just before an ostensibly identical SLICS shot. These spectra can be converted to a predicted time-of-flight for the following SLICS laser shot, giving the red and blue curves in the plot at right. These can them be compared with the shape of the time-of-flight distribution measured with the pTOF detector, which is green.

For the future it will be vital to have extremely reproducible energy spectra from shot-to-shot, as well as a “quasi-monoenergetic” spectra that allow us to separate protons and deuterons using the pTOF detector, with maximum suppression of heavier ions in the TNSA pulse.

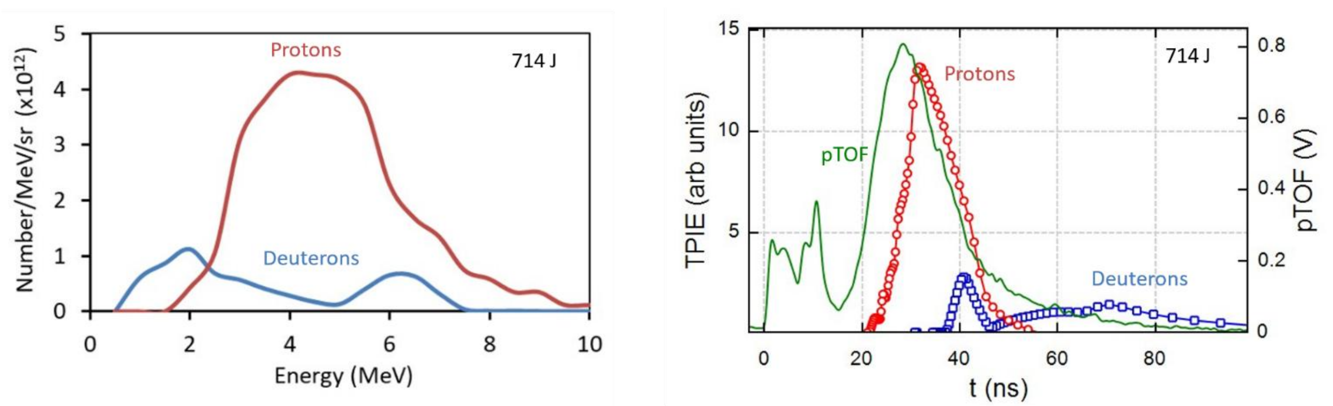

Figure 8. The TPIE-measured energy spectra (left) for protons and deuterons from 714 J shot 43434. These energy spectra can be converted to predicted TOF spectra, and compared to the measured pTOF spectrum from 714 J SLICS shot 43436. Since the pTOF light output is not normalized, the spectra have been scaled so the shape can be compared.

Figure 9 compares the measured and predicted ^{8}Li yield per Li atom, scaled so that all the measurements are at a lithium target distance of 100 cm. The error bars on the measured values primarily result from the uncertainty in the target thickness, which was assumed to be 15%. This systematic uncertainty was estimated from two sources. First, three thickness measurements were made at SUNY Geneseo across the face of each target, and the measured thicknesses were found to vary by an average of 9%. Second, the $^7Li(p,\alpha)^4He$ reaction at 1.5 MeV was used to measure the thickness, as shown in Figure 10. Given the disagreement between previous cross section measurements at similar backward angles, an uncertainty of 12% was used.

For the predicted yield calculation, the target thickness was assumed to be exact, and the yield was calculated using the ENDF $^7LI(d,p)^8Li$ cross section distribution, as shown in Figure 10. The measured cross section distributions vary significantly from the ENDF evaluated value, leading to a systematic uncertainty of 25% being applied to the predicted yield.

Several conclusions can be drawn from Figure 9. The predicted yields for the laser shot with energy around 730 J seems to show fair agreement with the measured yield. Examination of the corresponding TPIE deuteron energy distributions for these shots reveals that these were also similar. This agreement between predicted and measured yield might then be an indication that the deuteron energy distribution was also the same for the corresponding SLICS laser shot.

For the laser shots with energy near 370 J, there is one outlier deuteron energy distribution, from shot 43447. Later it was discovered that the laser target for this shot was much older than the other targets, created a year earlier. The target for laser shot 43431 was bent, and so it may just be a coincidence that it gave a similar deuteron distribution to shot 43425.

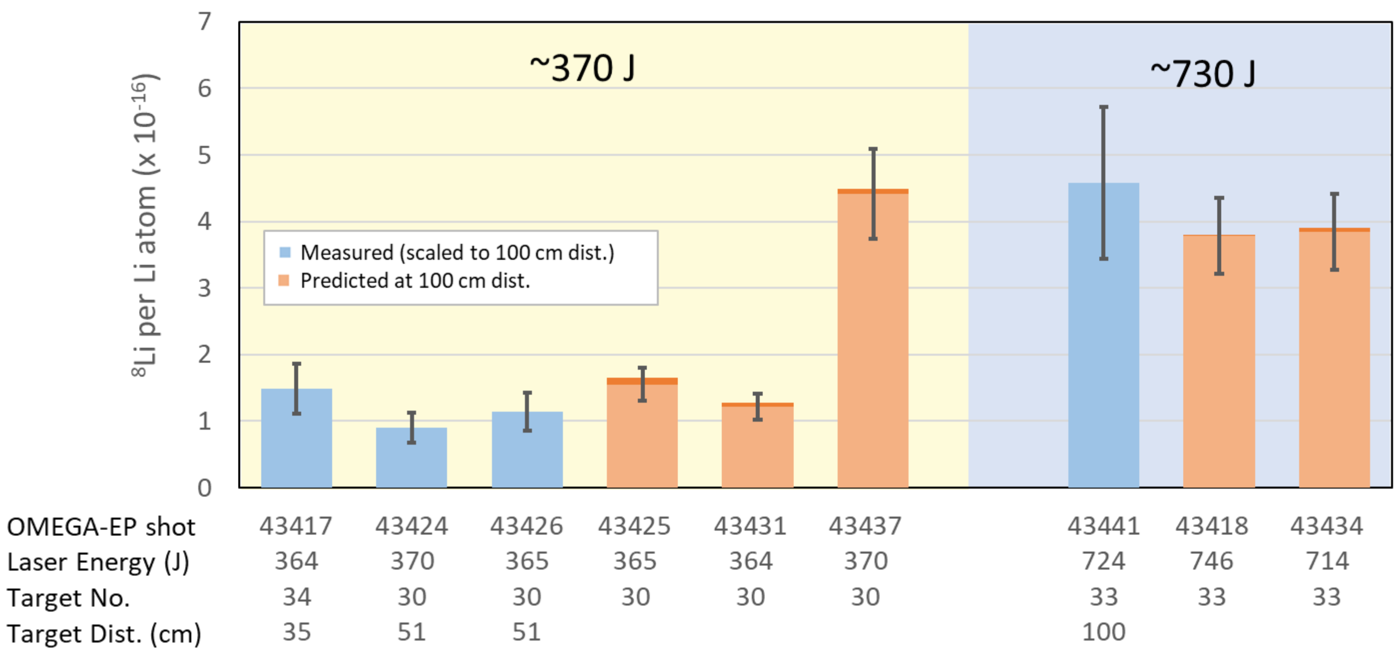

Figure 9. Comparison of the measured (blue) and predicted (orange) ^8Li yield per Li atom. The measured values have been scaled so that the distance to the lithium target is 100 cm. The predicted yields were calculated using TPIE deuteron energy distributions for laser shots with approximately the same laser energy as the SLICS shot, and have been corrected for target thickness. The darker region at the top of the predicted yield bars shows the chance in the yield due to deuteron energy loss in the target. Most of the uncertainty in the measured yield per atom results from the uncertainty in the target thickness due to the spread in previously measured $^7Li(p,a)^4He$ cross sections, most of the uncertainty in the prediction is from the spread of previously measured $^7Li(d,p)^8Li$ cross sections.

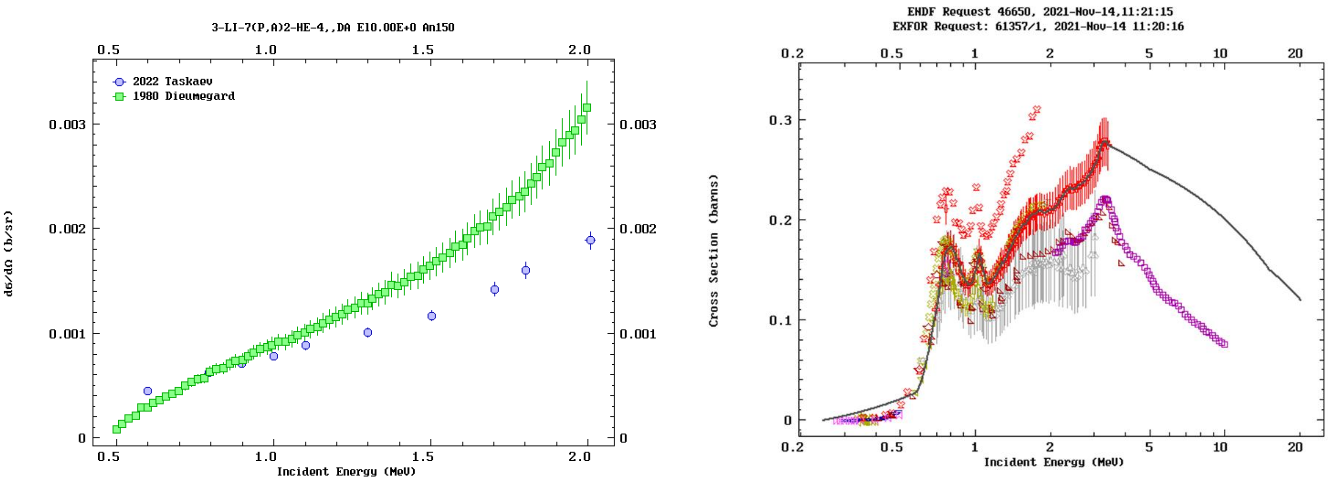

Figure 10. (Left) The differential cross section for the $^{7}Li(p,\alpha)^{4}He$ reaction at 168° from Taskaev et al. (blue circles) and at 150° from Dieumagard et al. (green squares). (Right) The total cross section for $^{7}Li(d,p)^{8}Li$ from all of the world's measurements (colored symbols), and the ENDF evaluated cross section (black line).

III. The Efficiency of the SLICS for Capturing and Detecting Radioactive ICF Products

One key datum that is needed before the SLICS can be used to measure thermonuclear cross sections for light ions is the likelihood of the product nuclei implanting or sticking to the getter foil just upstream of the face of the detector.

In this type of direct-drive ICF experiment, lasers strike a target capsule that has been filled with deuterium or tritium and doped with a material of interest, causing it to implode and nuclear reactions to begin. For example, in an experiment to measure $^{6}Li(t,p)^{8}Li$, the target would be filled with tritium and doped with ^{6}Li. After they are formed, the ^{8}Li product nuclei would travel outward through the expanding plasma. Some ions would have enough energy to punch through the plasma and implant in the getter, others would slow down, thermalize, recombine and form an expanding neutral gas which could then stick or react chemically with the getter. In either case, once they are on the getter foil the product nuclei decay and the resulting beta particles would be detected by SLICS.

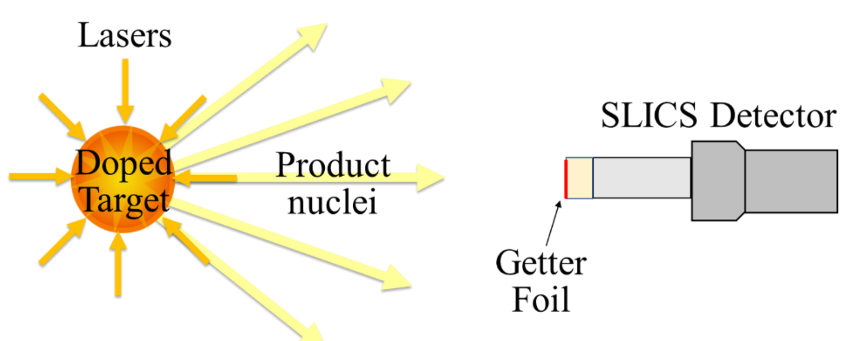

Figure 11. ICF SLICS experiment. Laser strike a doped target capsule, causing it to implode. Nuclear reactions occur which produce a radioactive product. These radioactive nuclei either implant or stick to a getter foil, where they decay and are detected by SLICS.

The type of reaction determines how much energy is available when the product nuclei are formed in an ICF implosion. For example, the $^{7}Li(t, \alpha)^{6}He$ reaction would yield ^{6}He nuclei up to 4.2 MeV, which would probably be more than enough to escape the plasma and implant in the getter foil. Conversely, a reaction like $^{3}H(t, \gamma)^{6}He$ would give ^{6}He nuclei with only about 40 keV; not enough to escape the plasma. Since ^{6}He is chemically an inert gas, most likely once these product nuclei slow down and form ^{6}He gas they would not stick to the getter at all. Other reactions, however, may product low-energy products that are chemically reactive and would stick to the getter. An example might be the $^{6}Li(t,p)^{8}Li$ reaction from above, which would produce only about 140 keV ^{8}Li. Lithium is very reactive and would no doubt stick to many getter materials.

If the fraction that sticks or implants in the foil can be determined, then, the number detected by SLICS allows the total amount of the product to be calculated. Since the amount of the reactants is known, this allows the reactivity (since there is a thermal distribution of ion energies) to be measured.

One way to measure fraction of the product nuclei that implant into the getter foil is shown in Figure 12. Primary neutrons from a high-yield DT ICF shot would strike a thin flat ring of either ^{8}Be or ^{11}B. These 14.1 MeV neutrons would create ^{6}He via $^{9}Be(n,\alpha)^{6}He$ or ^{8}Li via $^{11}B(n,\alpha)^{8}Li$, respectively. Because of the high neutron energy and the relatively large ^{4}He mass defect, the ^{6}He or ^{8}Li would have enough energy to escape from the thin target ring and implant into the SLICS getter. Since the neutrons are monoenergetic, and for a given ring radius the ^{6}He or ^{8}Li ions all scatter at the same angle, the ions will all be approximately monoenergetic. Figure 12 also shows the results of an MCNPX 2. 7 simulation tracking 10^{8} neutrons with forced collisions and source biasing for several ring diameters. Clearly as the ring diameter is increased, and therefore the scattering angle, the average energy decreases. Unfortunately, the largest possible scattering angle is 90° which sets the lowest energy that can be reached, and, since the spread of energies in the distribution also increases with the ring diameter, the method has only limited usefulness.

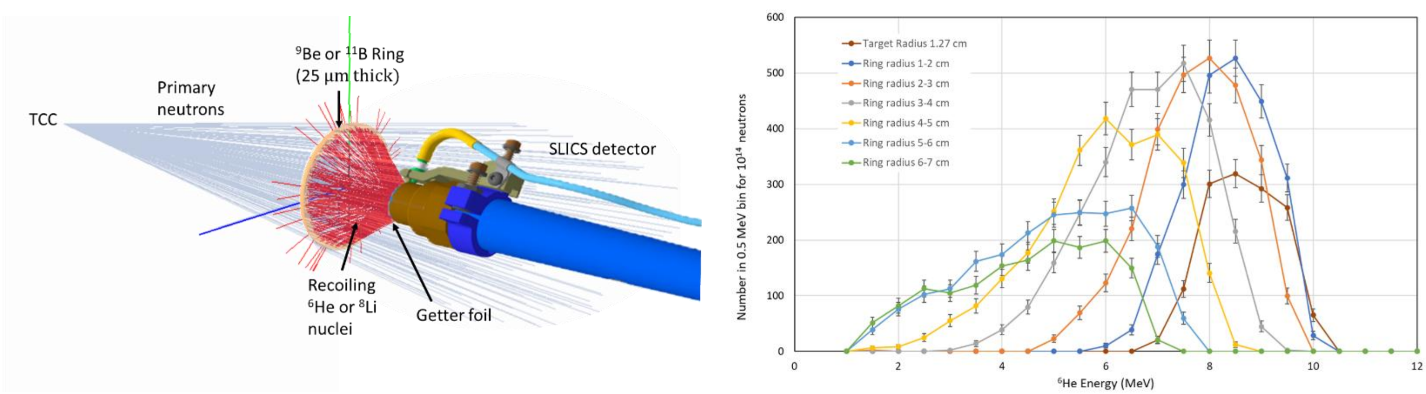

Figure 12. "Ring" method for measuring the fraction of ions implanted in the getter foil (left). Primary neutrons strike a thin flat ring of ^{8}Be or ^{11}B producing energetic ^{6}He or ^{8}Li ions respectively. These ions then implant into the SLICS getter foil and decay. An MCNPX simulation (right) shows the energy distributions of the ^{6}He ions as they strike the getter surface for various inside ring radii. For this simulation, the center of the 25 μm thick, 0.5 cm wide ring is 50 cm from target chamber center (TCC) and 5 cm from the getter. The simulation cuts off below 1 MeV.

Another, perhaps better way to measure fraction of the product nuclei that implant into the getter foil is shown in Figure 13. In this method, the primary neutrons from a high-yield DT ICF shot strike a thin flat disc of ^{8}Be or ^{11}B rather than a ring. The resulting ^{6}He or ^{8}Li that strike the SLICS getter foil are approximately monoenergetic since they are all traveling in the same direction. Air or some other gas is present between the target disc and the getter foil, so that the ions lose energy before implanting. Figure 13 presents the results of another MCNPX 2. 7 simulation tracking 10^9 neutrons with forced collisions and source biasing for different air pressures. As expected, the ion energy decreases with pressure. The width of the peak for each pressure is narrower than the widths achieved using the "ring" method, and, while they do widen, the peaks remain peaks all the way down to the lowest energies.

One interesting additional option with this method is that the ion energies can be reduced to zero by making the distance from the disc target to the getter foil equal to the ion range. In this case the ions will recombine and form neutral atoms, possibly allowing the fraction that stick chemically to be measured.

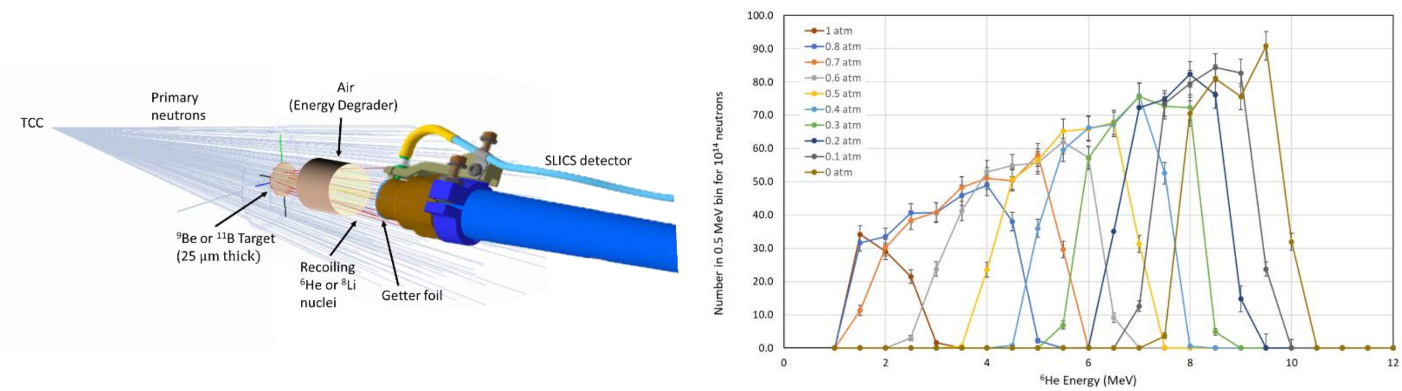

Figure 13. "Energy degrader" method for measuring the fraction of ions implanted in the getter foil (left). Primary neutrons strike a thin circular target of ^{8}Be or ^{11}B producing energetic ^{6}He or ^{8}Li ions respectively. These ions then lose energy traveling through air or some other gas used as an energy degrader before implanting into the SLICS getter foil and decaying. An MCNPX simulation (right) shows the energy distributions of the ^{6}He ions as they strike the getter surface for various degrader gas pressures. For this simulation, the center of the 25 μm thick, 0.5 cm wide ring is 50 cm from target chamber center (TCC) and 10 cm from the getter. The simulation cuts off below 1 MeV.

The final method, exhibited in Figure 14, is very similar to the "energy degrader" method described above, except in this case the neutrons come from the ^{7}Li(d,n)^{8}Be reaction when accelerated deuterons strike a natural lithium target. For 1.5 MeV deuterons, the neutrons scattered at 0˚ have nearly 16 MeV, so when they strike the Be or B target and produce ^{6}He or ^{8}Li, respectively, the product nuclei can have enough energy to escape from the target and implant into the getter foil.

There are several disadvantages to using an accelerator for this experiment, in contrast with ICF. First, the ions striking the getter are not monoenergetic, so the likelihood of implanting as a function of energy cannot be measured. This is because in order to get enough neutrons a thick lithium target must be used, resulting in a spread of neutron energies, and to get enough ^{6}He or ^{8}Li a thick Be or B target must also be used, which further broadens the outgoing ^{6}He or ^{8}Li energy distribution. The plot in Figure 14 shows the MCNPX simulated energy spectra of the ^{6}He and ^{8}Li ions reaching the getter for 1.5 MeV deuterons striking a 100 μm thick lithium target using a 200 μm thick Be or B target.

Even more troublesome, because the beam consists of a stream of deuterons and therefore a stream of neutrons rather than an extremely short 1 ns pulse, the product nuclei decay while they are being created. This means that the number of product nuclei reaches a maximum when the rate they are created equals the rate they are decaying. When this happens, the beam has to be cut off and the decays counted. In order to collect enough statistics, the beam therefore must be pulsed hundreds of times.

Despite these difficulties, it was decided the accelerator-based experiment was a worthwhile preliminary test of the idea and would allow us to put the apparatus through a shakedown test.

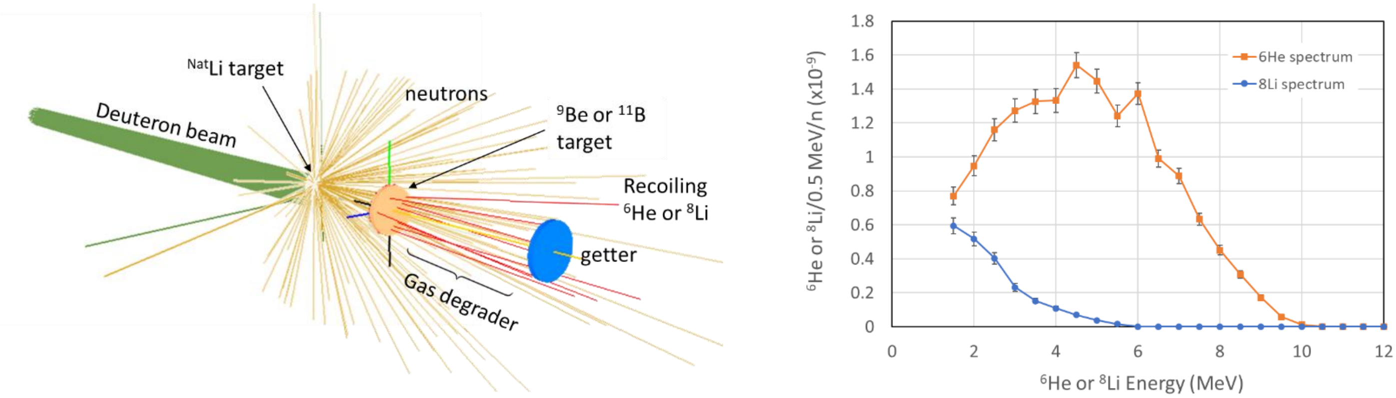

Figure 14. Accelerator method. In this method (left), a beam of deuterons strikes a natural lithium target producing high energy neutrons via the $^{7}Li(d,n)^{8}Be$ reaction. These neutrons then strike the ^{9}Be or ^{11}B target creating ^{6}He or ^{8}Li ions respectively. These ions can then escape the target and implant in the getter. Gas can be used as an energy degrader to control the energy of the ions. An MCNPX simulation (right) shows the energy distributions of the ^{6}He and ^{8}Li ions as they strike the getter surface. For this simulation, a 70 nA, 1.5 MeV deuteron beam struck the thick natural lithium target. The 200 µm thick beryllium or natural boron target was located 5 cm upstream of the getter foil. The simulation cuts off below 1 MeV.

IV. The Implantation Machine

During the summer of 2026 an apparatus to test the feasibility of these measurements was developed, which we have called the “implantation machine”, a schematic diagram for which is shown in Figure 15.

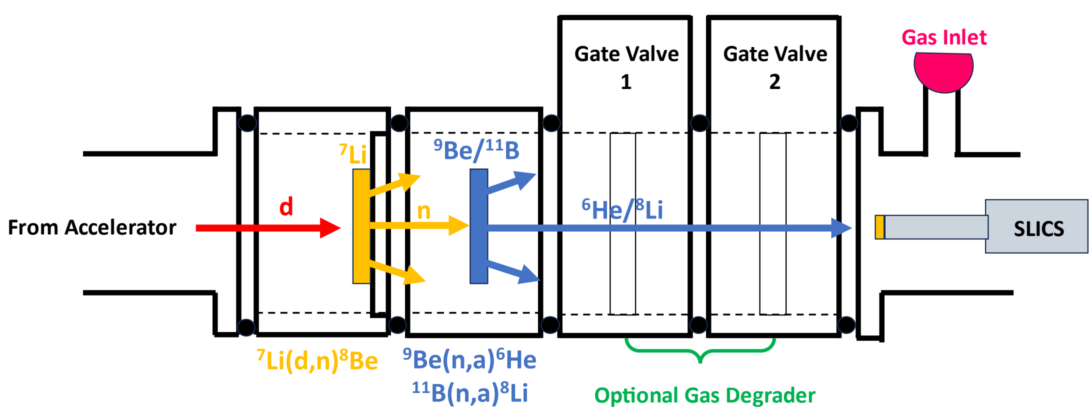

Figure 15. The implantation machine. Deuterons from the accelerator strike a thick lithium target, producing neutrons which then pass though a window leaving the accelerator vacuum chamber and entering the detector vacuum. They then strike a Be or B target to produce ^{6}He or ^{8}Li respectively. Gate valves can be used block the detection of beta particles from different regions: when gate Valve 1 is closed, betas from product nuclei stuck in the Be or B target are not counted, when Valve 2 is closed only the product nuclei implanted or stuck to the getter will be counted. The region between the Be or B target and the SLICS can be evacuated or filled with an energy degrading gas.

As shown in Figure 15, the "implantation machine" has a natural lithium film attached to a 2.75-inch conflat glass viewport with a thin layer of Dow Corning high vacuum grease. This target, which was struck by the deuteron beam, was within the accelerator vacuum system. Fixed with vacuum grease on the other side of the viewport, in a separate vacuum system, was a beryllium or boron target. Another flange, with an approximately 3.175 cm diameter o-ring grove was sealed to the glass viewport window using an AS-219 viton o-ring. The implantation machine can be evacuated using a rough pump, or held at a low pressure which can be monitored using a thermocouple gauge. The MTW version of SLICS is attached on the other side of the gate valves.

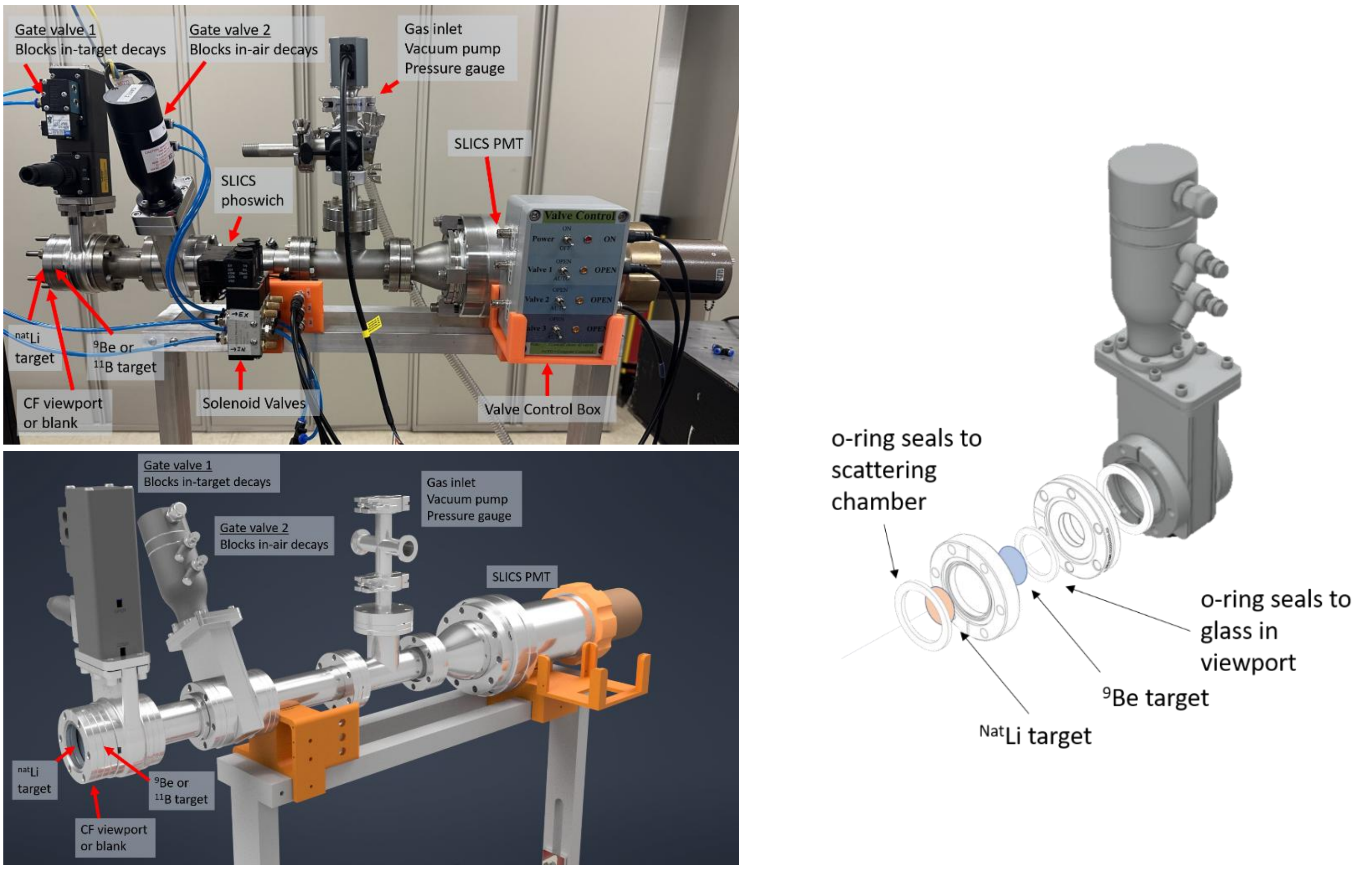

Figure 16. The "implantation machine" seals to the accelerator scattering chamber, and has its own separate vacuum system. The lithium target, which is hit by deuterons, is inside the scattering chamber. It produces neutrons which can penetrate through the viewport glass and strike the Be or B target. Pneumatic valves allow the ^{6}He or ^{8}Li to travel to the getter where they can implant (or not). They can also be used to stop beta articles.

Two 2.75-inch pneumatic conflat vacuum gate valves, a VAT Model 01032-UE44 and a Lesker Model SG0150PVCFM can be used to stop beta particles from the target from reaching the SLICS detector, or can be used to keep ^{6}He or ^{8}Li from implanting. Measurements of the opening and closing time for the valves were made using lasers that hit phototransistors, with a laser passing through each edge of the valve aperture, as shown in Figure 17. From this it was determined that the faster VAT valve begins closing about 60 ms after the GPIO control signal, and takes about 100 ms to close. The Lesker valve does not start closing until 450 ms after the GPIO signal and takes about 500 ms.

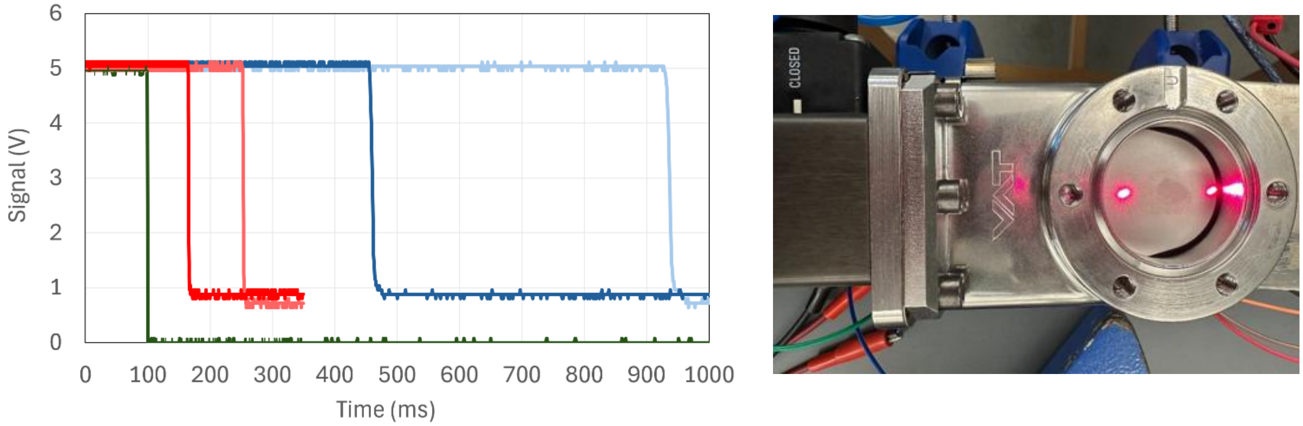

Figure 17. Lasers passing through each edge of the valve (right photo) to strike phototransistors were used to measure the time required (left plot) to close the Lester (blue) and VAT (red) gate valves. The GPIO control signal is black.

A new single-board computer (SBC) system was developed for the MTW SLICS detector, since the old Atomic Pi/Raspberry Pi 4 system is permanently stationed at LLE. The new SBC uses a Radxa X4 that includes both an Intel N100 and a Raspberry Pi RP2040 on the same board. As shown in Figure 18, the RP2040 controls the experiment, while the N100 is responsible for reading the data from the CAEN N6730SB digitizer. The accelerator beam is pulsed using a square wave from a signal generator that controls the current through one of the quadrupole focusing magnets. The RP2040 waits for the beam to go off, then starts the digitizer, which, for each phototube pulse, collects a sample every 2 ns for 400 samples. The RP2040 also sends 3.3 V GPIO logic signals to the circuit shown in Figure 19 that controls the solenoid valves to open and close the gate valves.

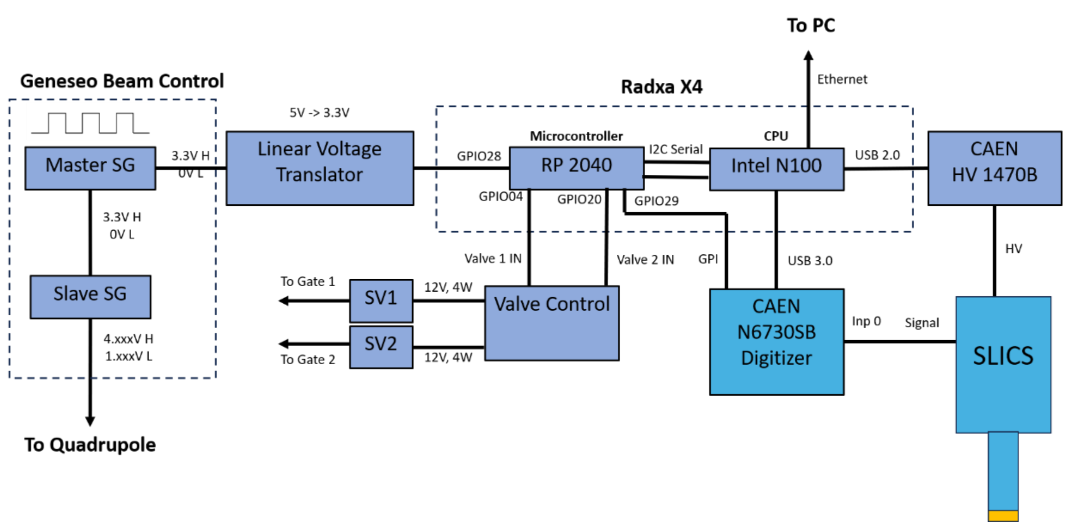

Figure 18. Block diagram of the new SLICS electronics. The square wave from the master signal generator controls the slave signal generator, which sets the voltage of one of the upstream focusing quadrupoles, allowing the beam to be pulsed by defocusing. When the beam turns off, the RP2040 microcontroller closes valves as desired and starts the data acquisition. The N100 CPU program then reads out the CAEN N6730SB digitizer. The system is controlled from another room via ethernet. The high voltage required for the PMT can be set remotely.

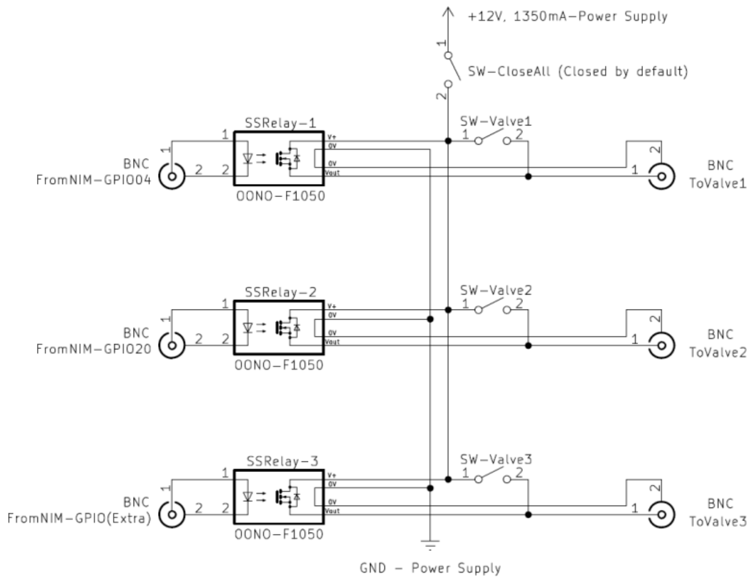

Figure 19. Valve control circuit. The CMOS 3.3 V logic signals from the RP2040 GPIO turn on or off the solid-state relays, which then power the solenoid valves that switch the compressed air that powers the vacuum gate valves. Switches allow the gate valves to also be opened and closed manually.

The experiment was carried out in July 2026 using the 1.7 MV Tandem Pelletron accelerator at SUNY Geneseo. A 15-100 nA beam of 1.5 MeV deuterons was initially allowed to strike the 102 µm thick metallic lithium target. The lithium was deposited on a 25 µm this stainless-steel substrate, which was stuck to the upstream surface of the 2.75 inch conflat viewport at the end of the 30R beamline. On the downstream side of the window, a 500 µm thick ^{9}Be target was attached using vacuum grease. The "implantation machine" was sealed to this viewport, but the gate valves were removed and the SLICS plastic scintillators were only a few centimeters from the viewport. After only a few pulses a very clear decay curve with an approximate half-life of 800 ms developed. Curiously, however, when the ^{9}Be target was removed and the experiment was repeated the same decay curve was measured. Subtracting the two curves gave a result consistent with zero.

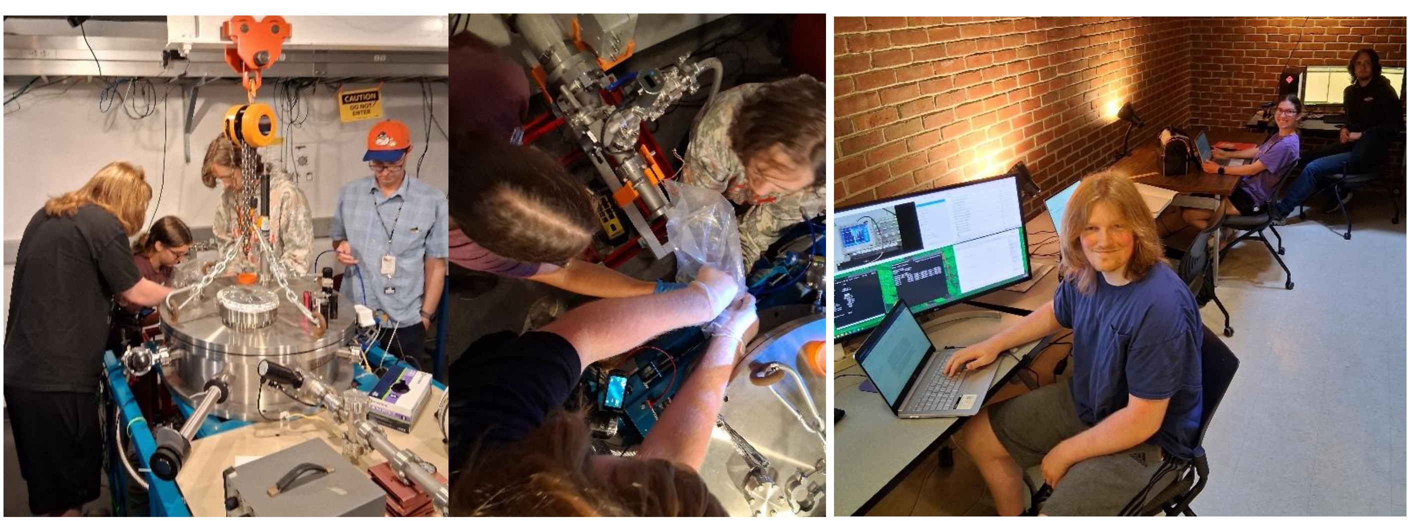

Figure 20. Houghton University students Sam Plymale, Olivia Ocker, and Dante Vara working with SUNY professor Dr. Charlie Freeman to install the lithium target (left, center). Houghton students controlling the data acquisition from the hallway "counting room" (right).

This result was puzzling because a nearly identical measurement in 2017 using the prototype detector gave a clean decay curve. One difference, however, was that in 2017 the neutrons were produced using $^{2}H(d,n)^{3}He$ with an energy of only about 5.2 MeV as compared to 15.9 MeV for the $^{7}Li(d,n)^{8}Be$ reaction. The borosilicate glass in the viewport contains boron, which can undergo the $^{11}B(n,a)^{8}Li$ reaction for neutrons above 7.2 MeV. Moreover, the $^{7}Li(d,p)^{8}Li$ reaction can also occur in the lithium target. Apparently, the 13 MeV betas from all these ^{8}Li were swamping the signal from the ^{6}He created in the ^{9}Be target by $^{9}Be(n,a)^{6}He$.

Because of this, the glass viewport was replaced with a 1.27 cm thick stainless-steel flange. Since the steel contains no boron, no ^{8}Li should have been created by $^{11}B(n,a)^{8}Li$. Any betas from the decay of the ^{8}Li created in the lithium target would be stopped in the steel, since the range of a 13 MeV beta is only about 0.9 cm. The experiment was repeated, unfortunately with exactly the same results.

It eventually turned out the primary problem was that the beam was not collimated, unlike in 2017. Deuterons were spraying the entire end of the scattering chamber, hitting the glass around the deuterated polyethylene target, and everything else nearby. When the beam was collimated, the results agreed with those from 2017 using the glass viewport and deuterated polyethylene.

At this point, several changes were made that seemed to solve these problems and allow the ^{6}He to be detected. First, the lithium target was replaced with a 100 μm thick boron carbide target (B_4C) in order to produce 14.85 MeV neutrons via $^{11}B(d,n)^{12}C$. Using boron for the target has several advantages over the lithium target. Both reactions have a cross section of about 0.4 barns at 1.5 MeV and both produce neutrons around 15-16 MeV in energy at 0°. The boron target however does not undergo $^{7}Li(d,p)^{8}Li$ so no ^{8}Li, with its 840 ms half-life and high-energy betas, will be produced by the primary deuteron beam. The $^{11}B(d,p)^{12}B$ reaction corresponding to $^{7}Li(d,p)^{8}Li$ produces ^{12}B which has a half-life of only 20 ms. These ^{12}B decays can be seen in the decay spectrum but do not interfere with the ^{6}He decay spectrum. While the $^{11}B(n,a)^{8}Li$ reaction still can occur with secondary neutrons to produce ^{8}Li as shown in Figure 21, the rate is much lower than $^{7}Li(d,p)^{8}Li$ with the primary deuteron beam.

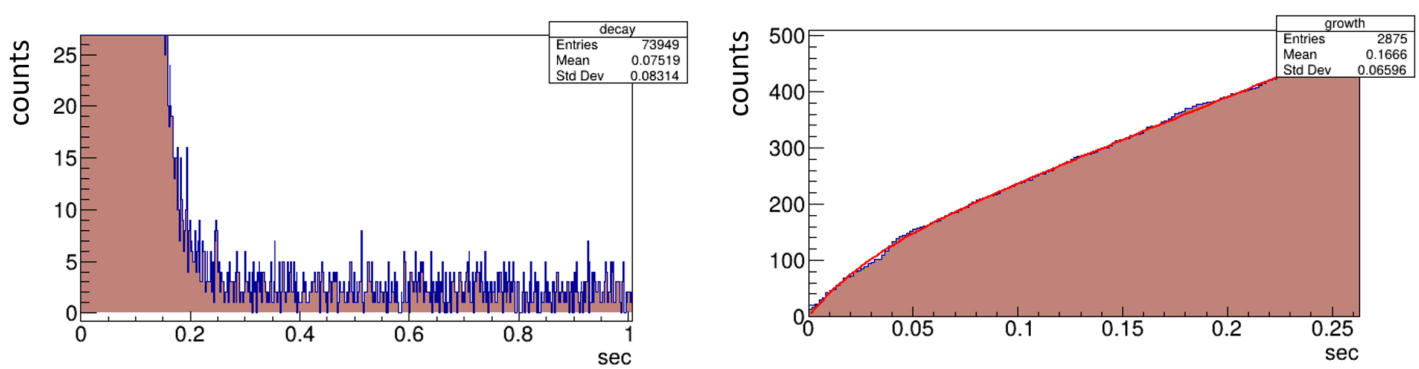

Figure 21. Zoomed in decay curve (left) shows short half-life exponential curvature that may be from ^{12}B created by $^{11}B(d,p)^{12}B$**.** This is for the 6.6 mm thick beryllium target for 200 pulses of the 17.8 nA 1.5 MeV deuteron beam striking a 100 μm thick B_4C target on the other side of a 1.27 cm thick steel blank. Integrating this curve and fitting (right) gives 88 ± 7 detected ^{12}B decays with fit half-life of 19.5 ± 3 ms and 11511 ± 38 counts/sec of background. The half-life of ^{12}B is 20.22 ms.

A typical 2D histogram is shown in Figure 22 for a 6.6 mm thick Be target about 1 cm from the SLICS. The events inside the red quaralateral were selected as good beta events, and histogrammed by their timestamps to give the decay curve in Figure 22. By monitoring the current flowing in the upstream focussing quadrupole used to pulse the beam, it was discovered that the quadrupole power supply lags the master signal generator square wave by about 125 ms. This accounts for the 150 ms of "beam on" recorded at the start of the decay curve. This time period was removed when fitting the decay and growth curves. Figure 23 compares the growth curve with the 6.6 mm Be target in and removed.

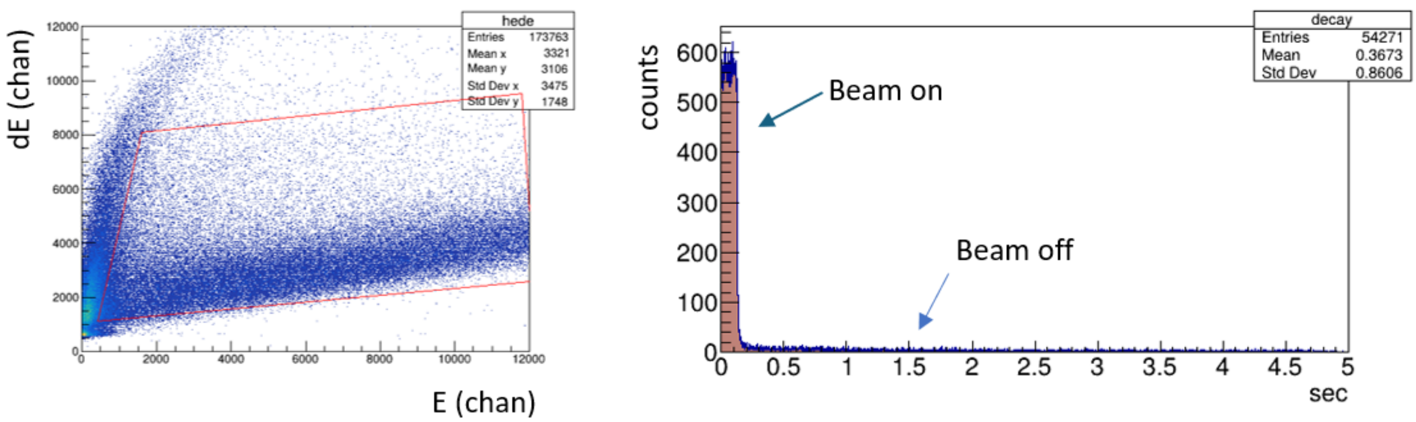

Figure 22. 2D dE-E histrogram (left) with the 6.6 mm thick beryllium target for 200 pulses of the 17.8 nA 1.5 MeV deuteron beam striking a 100 μm thick B_4C target on the other side of the 1.27 cm thick steel blank. The distance from the Be target to the SLICS scintillator was about 1 cm. The red box shows events selected as beta decays. The number of events inside the red box as a function of time is the decay curve (right). The magnet power supply decreased the quadrupole current approximately 150 ms after the square wave, hence the brief period when the SLICS detector was counting with the beam on.

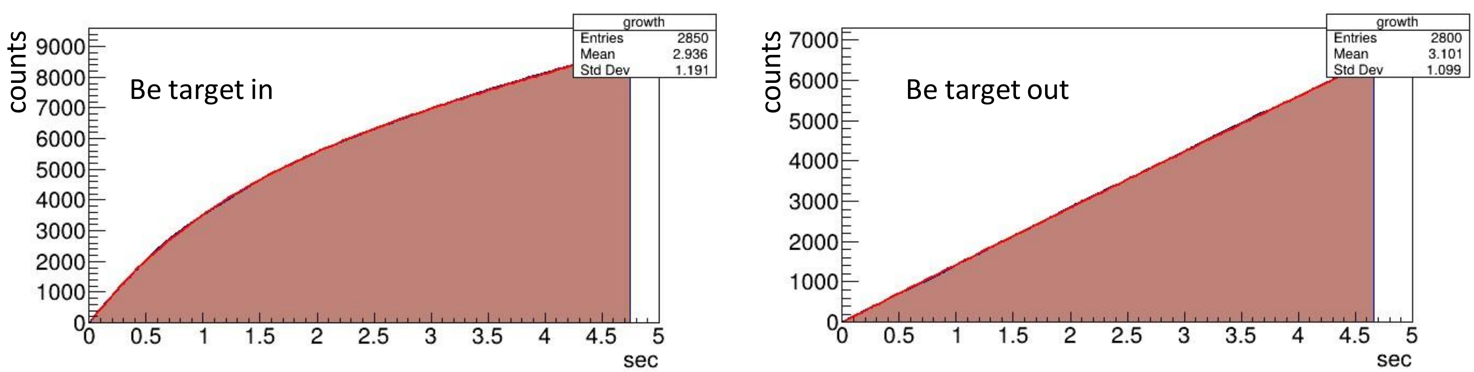

Figure 23. Integrating the decay curves from 200 ms on gives the growth curves above for both 6.6 mm thick beryllium target in (left) and out (right) for 200 pulses of the 17.8 nA 1.5 MeV deuteron beam striking the 100 μm thick B_4C target on the other side of 1.27 cm thick steel blank. The distance from the Be target to the SLICS scintillator was about 1 cm. For the "target in" run the red curve was fit to an exponential growth curve plus constant background, giving 4499 ± 26 ^6He decays detected, with a half-life of 8.1 ± 0.1 sec and a background rate of 943 ± 6 counts/sec. The empty target is consistent with a constant background of 1400 counts/sec.

The top row plots in Figure 24 show the decay and growth curves when the 6.6 mm thick beryllium was replaced with a 500 μm thick beryllium disc. At a distance of 1 cm from the SLICS, with this thinner target it was necessary to subtract the Be "target removed" background in order to reveal and fit the ^6He

decay and growth curves. In order to block beta particles from the Be target, allow or stop ^6He from reaching the detector, and to trap the gas used to slow down the ^6He ions, the gate valves needed to be inserted. The valves are relatively bulky -- inserting both of them with the intervening nipple would have added approximately 25 cm to the distance between the Be target and the SLICS. Instead, a single gate valve was inserted, which pushed the SLICS scintillator back to a distance of 5.6 cm, a little over five times as far, in order to produce the decay and growth curves in the bottom row of Figure 24.

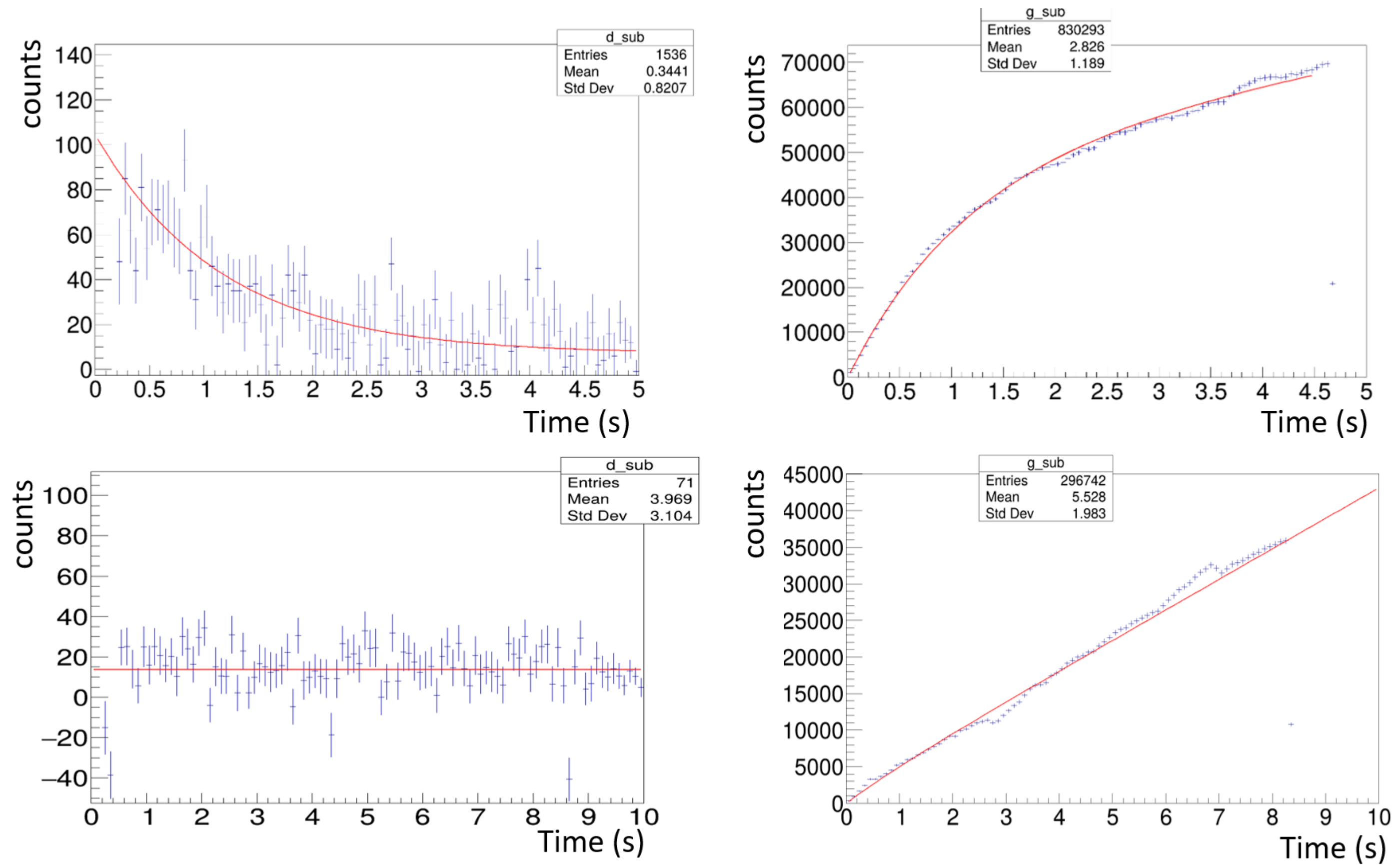

Figure 24. Subtracted target in minus target out decay (left) and growth (right) histograms for the 500 μm thick Be target with a Be to SLICS distance of 1 cm (top) and 5.6 cm (bottom). Fits with the 807 ms half-life of ^6He fixed are shown. At 1 cm the fit initial count rate was 98 counts in a 30 ms bin. At a distance of 5.6 cm, making the poor approximation that the rate falls like $1/r^2$, the expected initial rate would be only 3.1 counts per 30 ms, which would be undetectable without counting much longer.

The bottom-line conclusion from these experiments is that the current design for the implantation machine will not work with an accelerator-based neutron source for several reasons. The chief problem is that the distance between the neutron production target, the beryllium target, and the SLICS detector are too great to allow usable statistics to be collected relative to the background. For a 20 nA deuteron beam and with a 1.27 cm thick steel blank between the B_4C target and the Be target, the SLICS scintillators need to be no further from the 500 μm Be target than about 1 to 2 cm. Another problem is that gate valves are bulky and force the distance between the target and detector to be too large. Moreover, the thickness of the gate itself is too thin to effectively stop the 13 MeV endpoint betas from ^8Li.

In order to address these new design criteria, the "implantation machine 2.0" is shown below. In this design, the Be or B_4C target is attached to a fast solenoid retractor that allows it to be irradiated and produce ^{6}He or ^{8}Li but then retracted to prevent betas from ^{6}He or ^{8}Li stuck in the target (or other activation radiation) from reaching the SLICS. The ^{6}He or ^{8}Li that escape the target can travel through aerogel where they lose energy. Aerogel was selected because its properties are intermediate between gas and solid – allowing the ^{6}He or ^{8}Li to have a range on the order of 1-2 cm rather than 10 cm for gas or 10 μm for solids. In theory, only ^{6}He or ^{8}Li that implants in the getter (or stops in the aerogel) will be detected.

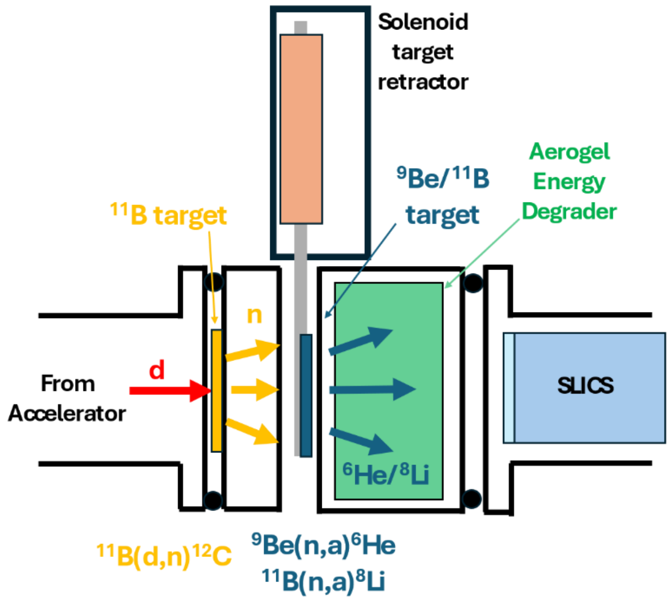

Figure 25. Revised design for the "Implantation Machine 2.0". The deuteron beam strikes a B4C target on the vacuum side of the steel conflat blank that seals the accelerator scattering chamber. Neutrons from the $^{11}B(d,n)^{12}C$ reaction the pass through the steel and strike a ^{9}Be ot ^{11}B target that is attached to a solenoid actuator that allows the target to be quicky (<100 ms) retracted or inserted. The ^{6}He or ^{8}Li that result from $^{9}Be(n,\alpha)^{6}He$ or $^{11}B(n,\alpha)^{8}Li$, respectively, then pass through an aerogel energy degrader with the appropriate density so that the range is at most a couple centimeters before they stick to or implant in the SLICS getter foil.

V. SLICS publications since summer 2025

A. K. Schwemmlein, M. Yuly, S. J. Padalino, G. Marcus, P. Gastis, B. Stanley, B. Wager, C. J. Forrest, and M. J. Rosenberg, "A Short-Lived Isotope Counting System (SLICS) to measure reaction cross sections producing light, beta-decaying nuclei on OMEGA," Rev. Sci. Instrum. 97, 043301 (2026).

VI. SLICS talks given since summer 2025

Mark Yuly, Charles Freeman, George Marcus, Stephen J. Padalino, Chad J. Forrest, Arnold Schwemmlein, Ben Stanley, and Panos Gastis, "Short Lived Isotope Counting System (SLICS) for Nuclear Experiments on OMEGA and OMEGA EP," 17th Annual OMEGA Laser Users Workshop, Laboratory for Laser Energetics, Rochester, NY, April 29, 2026.

Andrew Bo and Mark Yuly, "Deuteron and Triton Induced Light Ion Reactions Produced Via High-Power Short-Pulse Lasers," XLIV Annual Rochester Symposium for Physics Students, University of Rochester, April 18, 2026.

Mark Yuly, Andrew Bo, Charles Freeman, George Marcus, Stephen J. Padalino, Chad J. Forrest, Arnold Schwemmlein, Ben Stanley, and Christian Stoeckl, "Ten-Inch Manipulator-Based Short-Lived Isotope Counting System for Nuclear Experiments on OMEGA and OMEGA-EP," 67th Annual Meeting of the APS Division of Plasma Physics, Nov. 17-21, 2025.

Chad J Forrest, Ani Aprahamian, James DeBoer, Charlie Freeman, Panagiotis Gastis, Stephen Padalino, Mark Paris, Udo Schroeder, Arnold Schwemmlein, Ben Stanley, Christian Stoeckl, Mark Yuly, and Michael C Wiescher, "Tritium-induced nuclear reactions with light nuclei on the Omega Laser Facility," 67th Annual Meeting of the APS Division of Plasma Physics, Nov. 17-21, 2025.

P. Gastis, C. Forrest, S. Kuvin, H.-Y. Lee, U. Schroeder, A. Schwemmlein, B. Stanley, J. Winkelbauer, and M. Yuly, "Direct measurement of neutron-induced charged particle reactions relevant to fusion applications," 2025 Fall Meeting of the American Physical Society Division of Nuclear Physics, Chicago, IL, 17–20 October 2025.

VII. SLICS posters presented since summer 2025

B. Stanley, P. Gastis, E. Ruskov, C. J. Forrest, J. P. Knauer, J. Martinez, S. T. Ivancic, V. Gopalaswamy, A. K. Schwemmlein, H. Mcclow, M. J. Rosenberg, M. Yuly, S., G. Marcus, and S. J. Padalino, "Activation methods used to infer deuterium-deuterium neutron yields at the OMEGA laser facility," National Diagnostics Working Group, Sandia National Laboratory in Albuquerque, New Mexico, March 31 - April 2, 2026.

A. K. Schwemmlein, M. Yuly, S. J. Padalino, G. Marcus, P. Gastis, B. Stanley, B. Wager, C. J. Forrest, and M. J. Rosenberg, "A Short-Lived Isotope Counting System (SLICS) to measure reaction cross sections producing light, beta-decaying nuclei on OMEGA," National Diagnostics Working Group, Sandia National Laboratory in Albuquerque, New Mexico, March 31 - April 2, 2026.

Andrew Bo, Dante Vara, Samuel Plymale, Mark Yuly, Charles Freeman, George Marcus, Stephen J. Padalino, Chad J. Forrest, Arnold Schwemmlein, Ben Stanley, Christian Stoeckl, and Panos Gastis, "Initial Test of the Ten-Inch Manipulator-Based Short Lived Isotope Counting System," 17th OMEGA Laser User's Group Workshop, Laboratory for Laser Energetics, Rochester, NY, April 28-30,2026; XLIV Annual Rochester Symposium for Physics Students, University of Rochester, April 18, 2026, 67th Annual Meeting of the APS Division of Plasma Physics, Long Beach, CA, Nov. 17-21, 2025.

Dante Vara, Andrew Bo, Samuel Plymale, Mark Yuly, Michelle Woods, Silas Richardson, Chris Desiderio, Charles Freeman, George Marcus, Stephen J. Padalino, Chad J. Forrest, Arnold Schwemmlein, and Ben Stanley, "Measurement of deuteron- and proton-induced lithium reaction cross sections for SLICS detector efficiency calibration," 17th OMEGA Laser User's Group Workshop, Laboratory for Laser Energetics, Rochester, NY, April 28-30,2026; XLIV Annual Rochester Symposium for Physics Students, University of Rochester, April 18, 2026, 67th Annual Meeting of the APS Division of Plasma Physics, Long Beach, CA, Nov. 17-21, 2025.

VIII. SLICS undergraduate theses since summer 2025

Andrew O. Bo. "Deuteron and Triton Induced Light Ion Reactions Produced via High-Power Short-Pulse Lasers." B.S. thesis, (Houghton University, 2026).

This material is based upon work supported by the Department of Energy [National Nuclear Security Administration] University of Rochester "National Inertial Confinement Program" under Award Number(s) DE-NA0004144.

---

[1] Katelyn Cook, B.S. thesis, (Houghton College, 2019).

[2] Mark Yuly, Stephen Padalino, Micah Coates and Katelyn Cook, "A possible measurement of the 3H(t,γ)6He cross section at low energy," in Nuclear and Plasma Diagnostics for the EP-OMEGA and MTW Laser Systems, LLE Proposal for Subaward 416231-G (2016) (unpublished).

[3] Mark Yuly, Stephen Padalino, Micah Coates and Katelyn Cook, "A Phoswich Detector System to Measure the ^{3}H(t,α)^{6}He Cross Section using ICF" in Nuclear and Plasma Diagnostics for the EP-OMEGA and MTW Laser Systems, LLE Proposal for Subaward 416231-G (2017) (unpublished).

[4] Mark Yuly, Stephen Padalino, Emma Bruce, Katelyn Cook, and Sarah Hull, "Measuring Low Energy Nuclear Cross Sections using ICF," in Nuclear and Plasma Diagnostics for the EP-OMEGA and MTW Laser Systems, LLE Proposal for Subaward 416231-G (2018) (unpublished).

[5] Mark Yuly, Stephen Padalino, Tyler Kowalewski, Salvatore Ferri and Steven Raymond, "Inertial Confinement Fusion as a Tool to Study Fundamental Nuclear Science," in Nuclear and Plasma Diagnostics for the EP-OMEGA and MTW Laser Systems, LLE Proposal for Subaward 416231-G (2019) (unpublished).

[6] Mark Yuly, Stephen Padalino, Micah Christensen, Joshua Bowman, "Progress toward using ICF to measure light-ion nuclear cross sections" in Nuclear and Plasma Diagnostics for the EP-OMEGA and MTW Laser Systems, LLE Proposal for Subaward 416231-G (2020) (unpublished).

[7] Mark Yuly, Stephen Padalino, Adam Brown, Micah Christensen, Micah Condie, "Trapping and detecting trace radioactive isotopes produced in ICF implosions," in Nuclear and Plasma Diagnostics for the EP-OMEGA and MTW Laser Systems, LLE Proposal for Subaward 416231-G (2021) (unpublished).

[8] Tyler Kowalewski, "Inertial Confinement Fusion as a Tool to Study Fundamental Nuclear Science," B.S. Thesis (Houghton College, 2021).

[9] Mark Yuly, Stephen Padalino, Adam Brown, Andrew Hotchkiss, Chunsun Lei, Andrew Martin. "Trapping and detecting trace radioactive isotopes produced in ICF implosions," in Nuclear and Plasma Diagnostics for the EP-OMEGA and MTW Laser Systems, LLE Proposal for Subaward 416231-G (2022) (unpublished).

[10] Mark Yuly, Stephen Padalino, Noah Harley, Andrew Hotchkiss, Chunsun Lei, Andrew Martin. "A new technique for measuring light ion nuclear reactions using TNSA," in Nuclear and Plasma Diagnostics for the EP-OMEGA and MTW Laser Systems, LLE Proposal for Subaward 416231-G (2023) (unpublished).

[11] Andrew Martin, B.S. thesis, (Houghton University, 2023).

[12] Mark Yuly, Andrew Bo, Avery Belanger, Owen Fall, Stephen Padalino, and Charlie Freeman. "Nuclear physics using ultrafast high-power laser ion acceleration," in Nuclear and Plasma Diagnostics for the EP-OMEGA and MTW Laser Systems, LLE Proposal for Subaward 416231-G (2024) (unpublished).

[13] Mark Yuly, Andrew Bo, Sam Plymale, Dante Vara, Charlie Freeman, George Marcus, Stephen Padalino. "A Phoswich Detector System for Nuclear Measurements using ICF and TNSA." , LLE Proposal for Subaward 416231-G (2025) (unpublished).

[14] Andrew O. Bo, B.S. thesis, (Houghton University, 2026).

[15] B. Stanley, P. Gastis, E. Ruskov, C. J. Forrest, J. P. Knauer, J. Martinez, S. T. Ivancic, V. Gopalaswamy, A. K. Schwemmlein, H. Mcclow, M. J. Rosenberg, M. Yuly, S., G. Marcus, and S. J. Padalino, "Activation methods used to infer deuterium-deuterium neutron yields at the OMEGA laser facility," National Diagnostics Working Group, Sandia National Laboratory in Albuquerque, New Mexico, March 31 - April 2, 2026.

[16] P. Gastis, C. Forrest, S. Kuvin, H.-Y. Lee, U. Schroeder, A. Schwemmlein, B. Stanley, J. Winkelbauer, and M. Yuly, "Direct measurement of neutron-induced charged particle reactions relevant to fusion applications," 2025 Fall Meeting of the American Physical Society Division of Nuclear Physics, Chicago, IL, 17–20 October 2025.

[17] A. K. Schwemmlein, M. Yuly, S. J. Padalino, G. Marcus, P. Gastis, B. Stanley, B. Wager, C. J. Forrest, and M. J. Rosenberg, "A Short-Lived Isotope Counting System (SLICS) to measure reaction cross sections producing light, beta-decaying nuclei on OMEGA," Rev. Sci. Instrum. 97, 043301 (2026).

[18] Ani Aprahamian et al., J. Phys. G: Nucl. Part. Phys. **52** 063001 (2025).